NASA Technical Memorandum 106854
AIAA–95–0173

Two-Dimensional Imaging of OH in a Lean Burning High Pressure Combustor

R.J. Locke
NYMA, Inc.
Engineering Services Division
Brook Park, Ohio

Y.R. Hicks and R.C. Anderson
National Aeronautics and Space Administration
Lewis Research Center
Cleveland, Ohio

K.A. Ockunzzi
Ohio Aerospace Institute
Cleveland, Ohio

G.L. North
Vehicle Propulsion Directorate
U.S. Army Research Laboratory
Lewis Research Center
Cleveland, Ohio

Prepared for the
33rd Aerospace Sciences Meeting and Exhibit
sponsored by the American Institute of Aeronautics and Astronautics
Reno, Nevada, January 9–12, 1995

National Aeronautics and
Space Administration

TWO-DIMENSIONAL IMAGING OF OH IN A LEAN BURNING HIGH PRESSURE COMBUSTOR

R.J. Locke
NYMA, Inc.
NASA Lewis Research Center Group
Brook Park, Ohio 44142

Y.R. Hicks, R.C. Anderson
NASA Lewis Research Center
Cleveland, Ohio 44135

K.A. Ockunzzi
Ohio Aerospace Institute
Cleveland, Ohio 44142

G.L. North
Vehicle Propulsion Directorate
Army Research Laboratory
Cleveland, Ohio 44135

Abstract

Planar laser-induced fluorescence (PLIF) images of OH have been obtained from an optically accessible, lean burning high pressure combustor burning Jet-A fuel. These images were obtained using various laser excitation lines of the OH A←X (1,0) band for several fuel injector configurations with pressures ranging from 1013 kPa (10 atm) to 1419 kPa (14 atm). Non-uniformities in the combusting flow, attributed to differences in fuel injector configuration, are revealed by these images. Contributions attributable to fluorescent aromatic hydrocarbons and complex fuel chemistries are also not evident.

Introduction

The powerplants for the next generation supersonic aircraft are mandated to meet strict requirements for noise abatement, emissions reduction, and increased fuel efficiency. Efforts at NASA Lewis Research Center are directed towards reducing the powerplant emissions, specifically NO_x and unburned hydrocarbons (UHC). To lower engine emissions, an improved understanding of the combustion process at the requisite conditions of pressure, temperature, flow velocity, and fuel type is necessary. These extreme conditions pose unique challenges to all established diagnostic techniques.

Standard probe mechanisms have been used in the past to provide rudimentary knowledge of these flowfields. However, probes have proved to be an unsatisfactory diagnostic tool, since by nature they are time-averaged and non-spatially resolved. Additionally, probes adversely affect the measurement by disrupting the combusting flow resulting in potentially controvertible results. Conversely, laser-based diagnostic techniques have demonstrated the capability to supply nonintrusive quantitative information on such diverse parameters as species concentration, temperature, velocity, and pressure. Of these methods, planar laser-induced fluorescence (PLIF) offers the potential to acquire quantitative, temporally resolved, nonintrusive two-dimensional species, temperature and velocity measurements, all of which are of considerable interest and value to research in high pressure reacting flows, and advanced combustor design.

A large research base has been established in laser-induced fluorescence diagnostics of gaseous flows. The bulk of this work comprises point measurements, i.e., laser-induced fluorescence

(LIF)[1,2] and laser-saturated fluorescence (LSF)[3,4] from premixed and diffusion flames over a wide pressure range. Other work includes PLIF imaging of the flame front and various molecular species for premixed and diffusion flames at atmospheric pressures.[5,6] Species imaging with PLIF has also been extended to shock heated flows,[7,8] high pressure gaseous flames,[9,10] and internal combustion engines.[11] Additionally, recent experiments have captured PLIF images from high pressure spray flames.[12,13] In addition to flowfield imaging, much has been accomplished examining the effects of quenching at higher pressure.[14] Previous work has provided a valuable foundation for practical applications of PLIF imaging in an actual combustor operating at High Speed Research (HSR) conditions. However, until now, no single experiment has been performed that duplicates all conditions present in a HSR combustor. To that end, an optically accessible flame tube was designed and installed at NASA Lewis on a lean burning, air blast injection, Jet-A fueled test rig. Presented here are the first images of OH acquired from an optically accessible combustor duplicating HSR conditions.

Experimental Apparatus

Test Facility

The combustor test facility at NASA Lewis Research Center, used for this series of experiments, is designed for tests with inlet air pressures up to 1723 kPa, and non-vitiated air heated to as high as 866 K. The fuel injector scheme used in this study was that of lean direct injection (LDI), one of several fuel injection techniques under consideration for HSR applications. The LDI concept, described in detail elsewhere,[15,16] can be briefly summarized as a multiple source, fuel injection system with variable air swirl for flow stabilization and efficient fuel/air mixing.

Experimental Test Rig

The high pressure, high temperature test section used in these experiments is a variant of that illustrated schematically in figure 1. The flow area is a square section with dimensions of 7.62 cm x 7.62 cm. The combustion section is 74 cm long. For the purposes of these experiments, the optically accessible prevaporization section and the flame holder have been removed and the LDI fuel injector system installed. Additionally, the original combustor section was replaced with an identically sized, but optically accessible combustor housing, shown in figure 2. The optically accessible portion of the flame tube is located approximately 12 cm downstream from the fuel injector manifold.

Four polished, fused silica windows are arranged circumferentially and spaced 90° apart. The windows have a clear aperture of 5 cm (vertical dimension) by 3.8 cm (horizontal dimension) resulting in a 67% view of the flow cross section at this location. The fused silica windows are able to withstand the high combustion temperatures by means of thin film cooling each window. The nitrogen film cooling mechanism, as depicted in figure 2, provides no more than 10% of the aggregate combustor mass flowrate which has a maximum of 1.47 kg/sec. This nitrogen film prevents the windows from experiencing temperatures greater than 977 K at flow temperatures of 2033 K. The range of conditions that were sampled in this series of experiments is given in Table 1.

Table 1
Experimental Test Conditions

Parameter	Range
Inlet Temperature	811 K - 866 K
Rig Pressure	555 kPa - 1413 kPa
Equivalence Ratio (Φ)	0.41 - 0.53
Mass Flow Rate (air)	0.59 kg/s- 0.83 kg/s
Flow Velocity	24 m/s - 45 m/s
Fuel	Jet-A

Optical Systems

The laser and optical system used for acquiring the OH PLIF images is shown in figure 3. This system consisted of a Continuum Nd:YAG-pumped (NY-81C) dye laser (ND60), the output of which was doubled to provide the requisite UV radiation. The YAG laser 2nd harmonics provided approximately 800 mJ per pulse at 10 Hz. The dye laser, using R590 dye, produced pulses of 180 mJ at 564 nm. The dye laser output was frequency doubled to 282 nm by a nonlinear BBO crystal in a Continuum UVX frequency doubler/mixer in a UVT-1 configuration. The resultant doubled output was approximately 16 mJ per pulse with a bandwidth of approximately 1.0 cm^{-1}. The UV light was separated from the residual dye output by a pellin-broca prism. The dye laser was tuned to the specific rovibronic transitions of the OH A←X (1,0) band by directing the laser beam through the flame of a Bunsen burner and observing the fluorescence with a photomultiplier tube/boxcar averager system.

The doubled dye output was expanded and collimated to approximately 2 cm in diameter and directed through a series of high damage threshold, wavelength-specific UV mirrors to the test cell approximately 12 m distant. The total optical transport system is presented in figure 4. The laser beam, upon entering the test cell, was directed to the test section by means of an elaborate beam positioning system. This system comprises a 1.4 m long by 0.8 m wide 3-axis motorized rail table installed on the ceiling of the test cell. Each axis is independently operated and controls the axial and radial positioning of the laser beam.

The final segment of this positioning system was the sheet forming optics, which consisted of a spherical lens combination for beam sizing, coupled with a cylindrical lens with a 3 m focal length. The resultant focused laser sheet had dimensions of 33 mm x 0.3 mm. Laser energy, prior to entering the test section, was approximately 10 mJ distributed over the sheet and approximates a Gausian distribution. Laser energy at the laser focal volume within the test section is a function of the clarity and/or degree of degradation of the fused silica windows caused by combustion byproduct deposition or heat effects.

Image Collection

The fluorescence from OH formed within the flowfield was collected at 90° from the laser sheet with a 105 mm, f/4.5 Nikon UV lens attached to a Princeton Instruments, intensified CCD camera with a resolution of 576 x 384 pixels. The field of view of the camera approximated the collection window clear aperture of 5 cm vertical by 3.8 cm horizontal. The camera intensifier was synchronously triggered with the laser pulse and was gated for 50 ns.

A combination of a WG-305 Schott glass filter (2 mm) and a narrow band interference filter from Andover Corp. #313FS10-50 (2 mm), with a peak wavelength of 315 nm and a FWHM of 10.6 nm, was used to collect OH fluorescence while efficiently eliminating scattered laser light. The detection system was mounted to a 3- axis positioner obtained from Aerotech, Inc., which allowed repositioning of the detector to coincide with laser sheet placement.

Beam Delivery Control

Due to safety considerations, remote control was required for positioning of the laser sheet and detector systems. Motion control of up to 4 axes on the positioning table is effected by a Parker Hannifin Compumotor model 3000. Control of the Aerotech positioning system is by a Unidex model 11. The motion controllers were designed to be remotely operated from a 486 computer, using a standard IEEE communication interface. To reduce the complexity, a computer program was written to coordinate positioning of both the laser sheet and detector system. LabWindows/CVI, a product of National Instruments, was the software development tool used in writing the program.

This program allows the user to select which laser beam and detector configuration to be used for each test run. The user can also specify the type and orientation of each stage mounted in the test cell and how the stages are connected to the motion controllers. Based on these selections, the program controls the distance and direction that each stage moves. The user is able to position the laser sheet in terms of rectangular coordinates using fractions of millimeters. The program records the user's coordinates, as well as all test conditions. The user also is able to define an origin, so the coordinates entered correspond to the position of the laser beam in the test region. This origin is also recorded, so that it can be reproduced for the next test run, or in case of power failure.

Image Analysis

Princeton Instrument's WinView software running on a 486 PC was used to acquire and temporarily store all ICCD images. The images were subsequently transferred to and stored on an SGI Indigo workstation for further processing due to the Indigo's faster processing time and greater disk storage.

Processing on the SGI workstation was accomplished using the PV-WAVE software package, version 4.20, from Visual Numerics, Inc. PV-WAVE subroutines have been developed to read the WinView image format and convert each image into an array usable by PV-WAVE. For displays using a 256-color palette, the images are scaled so that the minimum is 0 and the maximum is 255. For the results presented herein, image processing includes background subtraction, removal of noise spikes and correction for laser beam profile nonuniformity.

Background subtraction effectively reduces the minimum pixel value for an image to near zero by subtracting from each image pixel value, the value of the corresponding pixel in a background image. Where a background image is not available the

image minimum value is subtracted from all pixels.

Removal of image noise spikes is necessary in these experiments due to their adverse affect upon any scaling routine. The cause of the spikes is unknown at present, but particulate emission and electrical noise on long cables from camera to acquisition electronics are under investigation as possible causes. The noise spikes take the form of an island of 1 or 2 pixels with a value much higher than surrounding pixels. The spike noise removal routine works by adjusting the value of all pixels whose value exceeds the threshhold value. The threshhold value depends on the image histogram such that the threshhold value is that value below which lie 98% of all pixel values. Each pixel value is changed to equal the threshhold value for all pixels whose original value exceeds the threshhold value.

Correction of images for laser beam nonuniformity requires knowledge of the beam intensity profile and knowledge of the location of the beam in each image. For these experiments, the intensity profile was measured using fluorescence from a polished fused silica dye cell (50 mm x 50 mm x 10 mm) filled with a concentrated R590 dye solution. Since the flame tube duct was inaccessible just prior to an experiment when the profile measurement was needed, the camera assembly was raised to place its line of sight above the flame tube so that the dye cell could be placed in the path of the laser sheet and at the same distance from the camera as the test location. A beam profile image was taken and was available to correct all images for that experiment. To correct images the beam intensity profile is taken to be a vector whose length is the same as an image row. The beam profile vector elements have values equal to the relative magnitude of the sum of all pixels in the image column corresponding to that vector element. The beam profile vector yields a good estimate of the beam profile; but knowledge of the location of the beam in the images is also required.

For these experiments, a direct measurement of the beam location was not available, so an indirect method was developed. For each image to be corrected an image profile vector was computed using the same image column summing method as in the case of the beam profile vector. The beam profile and image profile were plotted together on the same plot and the beam profile plot was shifted under operator control until an apparent match was obtained. The shifted beam profile was then used to correct the image. For future work a commercially available laser beam profile measurement system will replace the current dye cell technique. The new method is a Windows-based system which incorporates a 40 mm square diode array fitted with a fluorescent plate, accessing the 180-400 nm UV region. The two-dimensional array, located on the bottom of the test section at the laser sheet exit window, will be synchronously triggered with the intensified camera, thus providing energy normalization for each PLIF image.

Results

All PLIF images were obtained with the camera remotely positioned to center its field of view on the collection window, with the illuminated flowfield at its focus. The upstream edge of the windows corresponds to a position approximately 13 cm downstream of the fuel injector exit. Equilibrium code calculations[17] for LDI injection and HSR conditions of Jet-A fuel, 1034 kPa, 811 K inlet air, and, Φ=0.47 (f/a = 0.032), have predicted OH concentrations of approximately 300 ppm in the flame zone. The code also predicted that the range of equivalence ratios and pressures examined in this study would not cause significant change in the OH concentration.

All PLIF images were attained via the use of one of three rovibronic transitions of the OH A←X (1,0) band: $R_1(1)$ 281.458 nm, $R_1(10)$ 281.591 nm and $Q_1(1)$ 281.970 nm. In all cases, the laser sheet passes vertically, from top to bottom. The flow passes from left to right.

The images obtained in this study are all qualitative in nature. The results presented here are for technique application validation purposes only. No attempt was made to derive a quantitative number for OH concentration. The OH images portray relative fluorescent yields only. Extraction of quantitative concentration distributions for OH and NO, as well as flowfield temperature distribution maps, will be attempted in future experiments when a second tunable dye laser is installed.

Unless otherwise stated, all images presented herein have been subjected to background subtraction and pixel noise spike removal routines. With the exception of figure 8, each image within a figure has been normalized to that image within the figure with the highest pixel value. Only figure 5 has been normalized for laser sheet energy distribution.

Figure 5 shows a comparison of an uncorrected, single-shot OH PLIF image (left) with the same image corrected for laser sheet energy distribution (right). The image was acquired for 9 point LDI with 45° swirl at 1034 kPa (10 atm), $\Phi = 0.53$, (f/a = 0.036) and $R_1(10)$ excitation An obvious nonuniform OH distribution is evident in both the uncorrected and corrected images. The drop-off of OH fluorescent signal intensity suggests that the windows are located at the trailing edge of the reactive region.

Figure 6 gives a comparison of resonant and off-resonant, ten shot averaged OH PLIF images for 9 point LDI with 60°/45° swirl at 1034 kPa and Φ= 0.53 (f/a = 0.036). Excitation of the resonant image was accomplished via the $R_1(10)$ line at 281.591 nm, while the off resonant excitation was at 281.01 nm. These images were uncorrected for laser sheet energy distribution.

The off-resonant image in figure 6 shows no evidence of either elastically scattered laser light or contributions attributable to complex fuel chemistries and/or polycyclic aromatic hydrocarbons (PAH). This is of considerable importance due to the strong concerns relating to complex hydrocarbon pyrolysis chemistry associated with non-premixed flames at elevated pressure.[18]

Figure 7 is a comparison of two OH PLIF images obtained with different resonant wavelength excitation for 9 point LDI with 60°/45° swirl at 1034 kPa, 866 K inlet air and $\Phi = 0.53$. The images were acquired by tuning the dye laser to the different lines while maintaining uniform flow conditions. The left image, excited with R_1 (1), shows no indication of laser sheet attenuation, while the right image, excited with $Q_1(1)$, shows strong evidence of attenuation. The plots immediately below each image in figure 7 give the relative pixel intensity from bottom to top along the vertical lines drawn at the same position through each respective image. The left-hand plot for $R_1(1)$ excitation again displays no evidence of laser sheet attenuation. Conversely, the right-hand plot shows significant lessening of intensity, on the order of 60%. This observation emphasizes the importance of judicious selection of excitation lines for these flow conditions.

Figure 8 contrasts two PLIF images for different LDI fuel injector swirl angles, taken at the same conditions, 1034 kPa, 866 K inlet air, and $\Phi = 0.53$. Each image is a ten shot average obtained from exciting the $R_1(10)$ transition. The figure on the left, with 45° swirl, is similar to the image presented in figure 5, also with 45° swirl, and all other images obtained with this configuration. The image on the right, using 60°/45° swirl, displays a more uniform flowfield, a manifestation substantiated by all images acquired with this configuration.

From figures 8 and 5, it is immediately apparent that with 45° injection swirl, the greater fraction of OH, and hence, higher flow temperatures, is located along the upper and lower walls of the combustor. This injector configuration was previously presumed to provide a uniform flowfield such as seen in images acquired from the 60°/45° configuration. The findings here have shown that the ability to disclose the actual flowfield via species/temperature distributions is of significant value in providing feedback to actual combustor design.

Figure 9 is a comparison of OH PLIF images acquired at the same flow conditions but at different equivalence ratios. The flow conditions for all three images were: 866 K inlet air, 1413 kPa (14 atm), flow velocity of 33.5 m/s (110 ft/s),and a mass flow rate of 0.83 kg/s. Laser excitation was achieved via the $R_1(10)$ transition at 281.591 nm. Each image was normalized for WinView autoscaling routine differences, thus presenting an accurate representation of the relative fluorescence intensity. As expected, the OH fluorescence intensity dramatically diminishes with decreasing equivalence ratio.

Conclusions

The results reported here demonstrate the viability of the planar laser-induced fluorescence diagnostic technique in applications to actual high pressure/high temperature combustors. PLIF images of OH were obtained at a range of test conditions duplicating those to be experienced in future HSR-type combustors. Quenching was shown to play no major role in hindering the capture of the OH images. However, laser sheet attenuation was shown to be a important factor in excitation transition selection.

The PLIF imaging technique has proved to be a valuable tool to combustor designers. Its ability to portray the relative OH species concentration distribution, and hence the temperature distribution in the flow field, provides a unique opportunity to view actual combustion flowfield at these conditions.

The fused silica windows suffered no physical damage during the entire study. Some deposition of

material onto the inner window surfaces did occur at test conditions near the lean stability limit (Φ ~ 0.39). The amount, however, was insignificant and burned off at elevated temperatures. Windows were typically cleaned during routine test rig internal examinations, and during hardware configuration changes. Towards the end of the study, some minor warping of the thin film cooling lips was experienced. This warping was attributed to the loss of protective ceramic coating thereby exposing the Wasp-alloy material of the lips to flow temperatures. Minor repairs, and a reapplication of the ceramic coating, corrected the warpage.

Future Considerations

Research efforts using the optically accessible combustor are on-going and are now directed to the measurement of other species of interest as well as attempting to ascertain a flowfield temperature distribution. Additionally, certification for higher temperature and pressure operation of the optically accessible housing is also being sought.

References

1. Heard, D.E., Jeffries, J.B., Smith, G.P., and Crosley, D.R., "LIF Measurements in Methane/Air Flames of Radicals Important in Prompt-NO Formation," *Combustion and Flame*, **88**, pp.137-148, 1992.
2. Reisel, J.R., Campbell, C.D., and Laurendeau, N.M., "Laser-Induced Fluorescence Measurements of Nitric Oxide in Laminar $C_2H_6/O_2/N_2$ Flames at High Pressure," *Combustion and Flame*, **92**, pp 485-489, 1993.
3. Lucht, R.P., Sweeney, D.W., and Laurendeau, N.M., "Laser-Saturated Fluorescence Measurements of OH Concentration in Flames," *Combustion and Flames*, **50**, pp. 189-205,
4. Carter, C.D., King, G.B., and Laurendeau, N.M., "Quenching- Corrected Saturated Fluorescence Measurements of the Hydroxyl Radical in Laminar High-Pressure $C_2H_6/O_2/N_2$ Flames," *Combust. Sci. Tech.*, **78**, p. 247, 1991.
5. Hanson, R.K., "Combustion Diagnostics: Planar Imaging Techniques,"*Twenty-First Symposium (International) on Combustion*, The Combustion Institute, pp. 1677-1691, 1986.
6. Paul, P.H., Meier, U.E., and Hanson, R.K., "Single-Shot, Multiple-Camera Planar Laser Induced Fluorescence Imaging in Gaseous Flows," AIAA Paper, No. 91-0459, 29th Aerospace Sciences Meeting, Reno, Nevada, January, 1991.
7. Allen, M.G., Parker, T.E., Reinecke, W.G., Legner, H.H., Foutter, R.R., Rawlins, W.T., and Davis, S.J., "Fluorescence Imaging of OH and NO in a Model Supersonic Combustor," *AIAA Journal*, **31**, No. 3, pp. 505-512, 1993.
8. Seitzman, J.M, Palmer, J.L., Antonio, A.L., Hanson, R.K., DeBarber, P.A., and Hess, C.F., "Instantaneous Planar Thermometry of Shock-Heated Flows Using PLIF of OH," AIAA Paper, No. 93-0802, 31st Aerospace Sciences Meeting and Exhibit, Reno, Nevada, January, 1993.
9. Battles, B.E. and Hanson, R.K., "Laser-Based Measurements of OH in High Pressure CH_4/Air Flames," AIAA Paper, No. 91-1494, 22nd Fluid Dynamics, Plasma Dynamics & Lasers Conference, Honolulu, Hawaii, June, 1991.
10. Battles, B.E., Seitzman, J.M., and Hanson, R.K., "Quantitative Planar Laser-Induced Fluorescence Imaging of Radical Species in High Pressure Flames," AIAA Paper, No. 94-0229, 32nd Aerospace Sciences Meeting and Exhibit, Reno, Nevada, January, 1994.
11. Andresen, P., Meijer, G., Schluter, H., Voges, H., Koch, A., Hentschel, W., Oppermann, W., and Rothe, E., "Fluorescence Imaging Inside an Internal Combustion Engine Using Tunable Excimer Lasers," *Applied Optics*, **29**, No. 16, pp. 2392-2404, 1990.
12. Allen, M.G., Davis, S.J., and Donohue, K., "Species and Temperature Imaging in Liquid-Fueled Spray Flames," AIAA Paper, No. 90-2440, AIAA/ASME/SAE/ ASEE 26th Joint Propulsion Conference, July 1990.
13. Koch A., Chryssostomou, A., Andresen, P., and Bornscheuer, W., "Multi-Species Detection in Spray Flames With Tunable Excimer Lasers," *Applied Physics B*, **56**, p. 165, 1993.
14. Paul, P.H., "A Model for Temperature-Dependent Collisional Quenching of OH A $^2\Sigma^+$," *J. Quant. Spectrosc. Radiat. Transfer*, **51**, No. 3, pp. 511-524, 1994.
15. Alkabie, H.S., Andrews, G.E. and Ahmad, H.T., "Lean Low No_x Primary Zones Using Radial Swirlers," ASME Paper 88-GT-245, 1988.
16. Hussain, U.S., Andrews, G.E., Cheung, W.G., and Shahabadi, A.R., "Low No_x Primary Zones Using Jet Mixing Shear Layer Combustion," ASME Paper, 88-GT-308, 1988.

17. Gordon, S. and McBride B.J., "Computer Program for Calculation of Complex Chemical Equilibrium Compositions, Rocket Performance, Incident and Reflected Shocks, and Chapman-Jouget Detonations," *NASA SP-273*, 1971.
18. Allen, M.G., McManus, K.R., and Sonnenfroh, D.M., "PLIF Imaging Measurements in High-Pressure Spray Flame Combustion," AIAA Paper No. 94-2913, AIAA/ASME/SAE/ASEE Joint Propulsion Conference, Indianapolis, Indiana, June 1994.

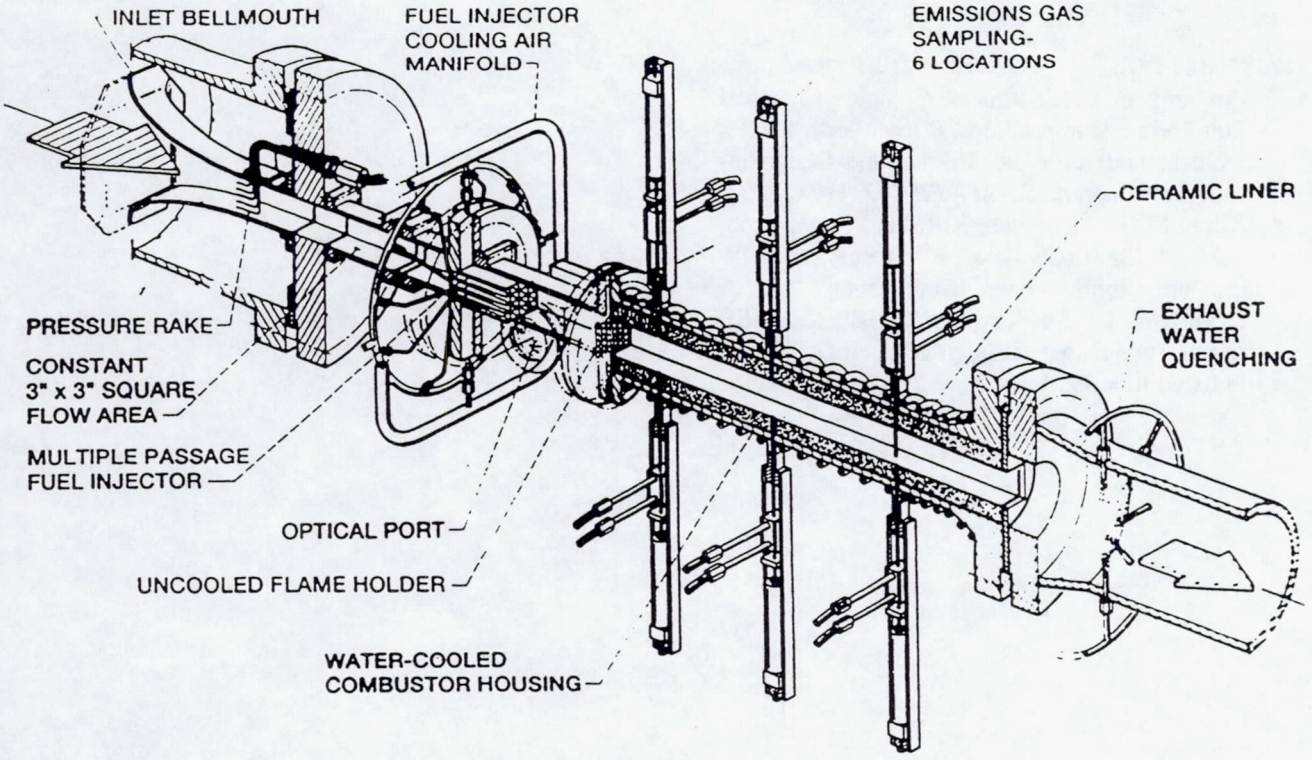

Fig. 1 High pressure, high temperature square cross section flame tube.

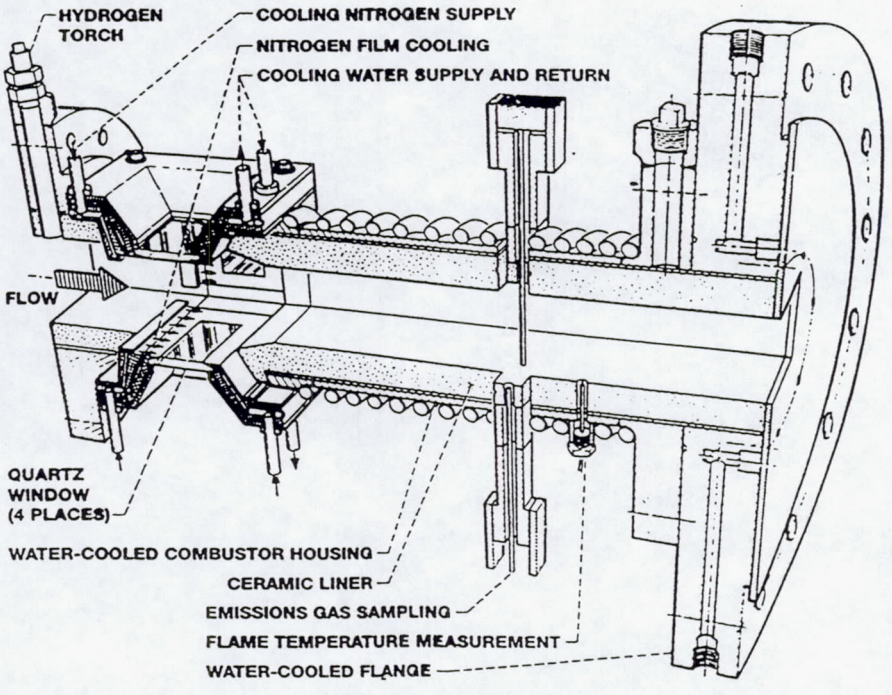

Fig. 2 Thin film cooled, optically accessible flame tube.

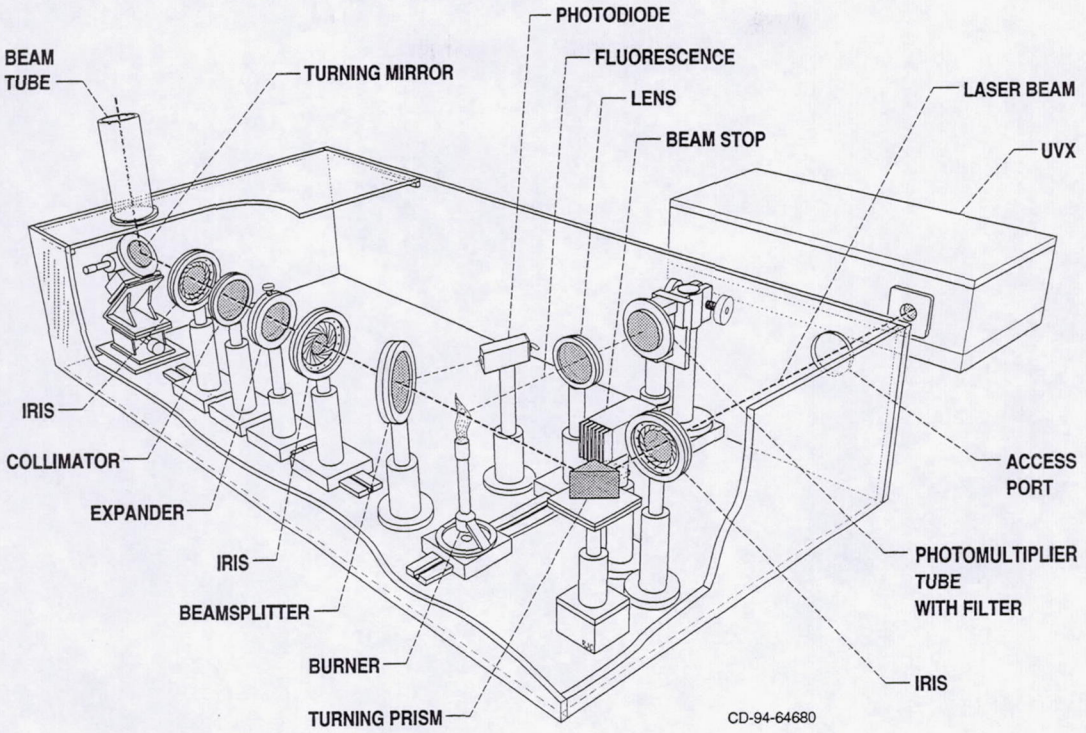

Fig. 3 Beam Transport System Optics

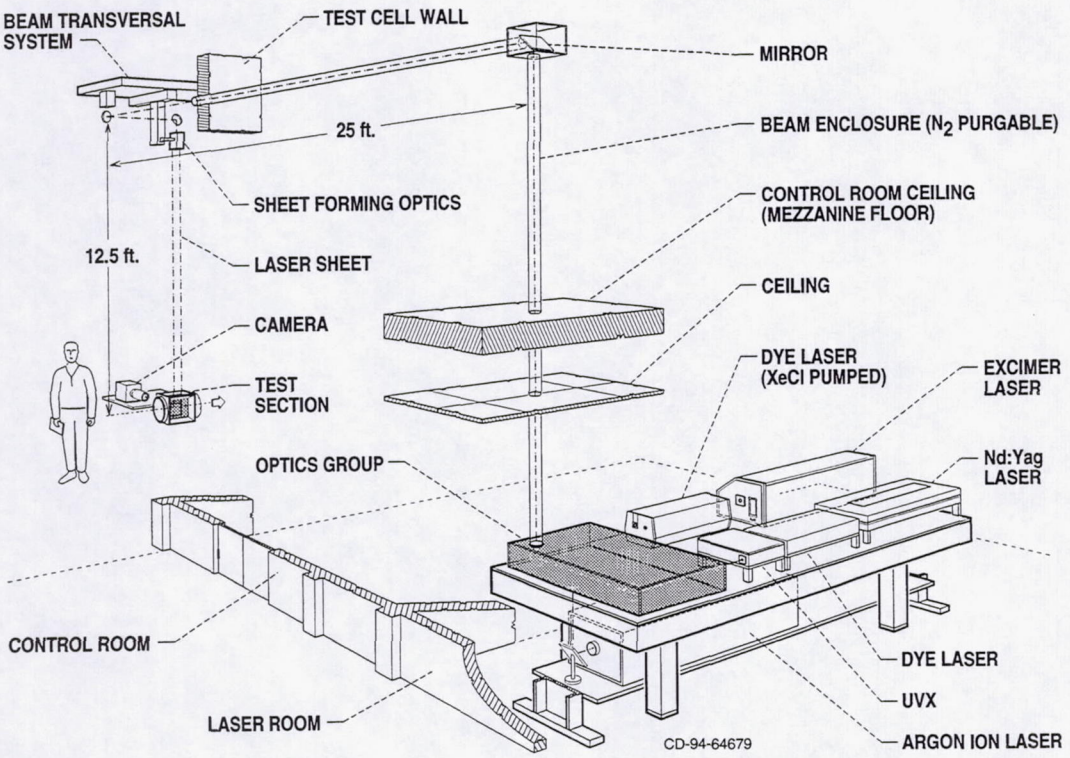

Fig.4 Beam Transport System

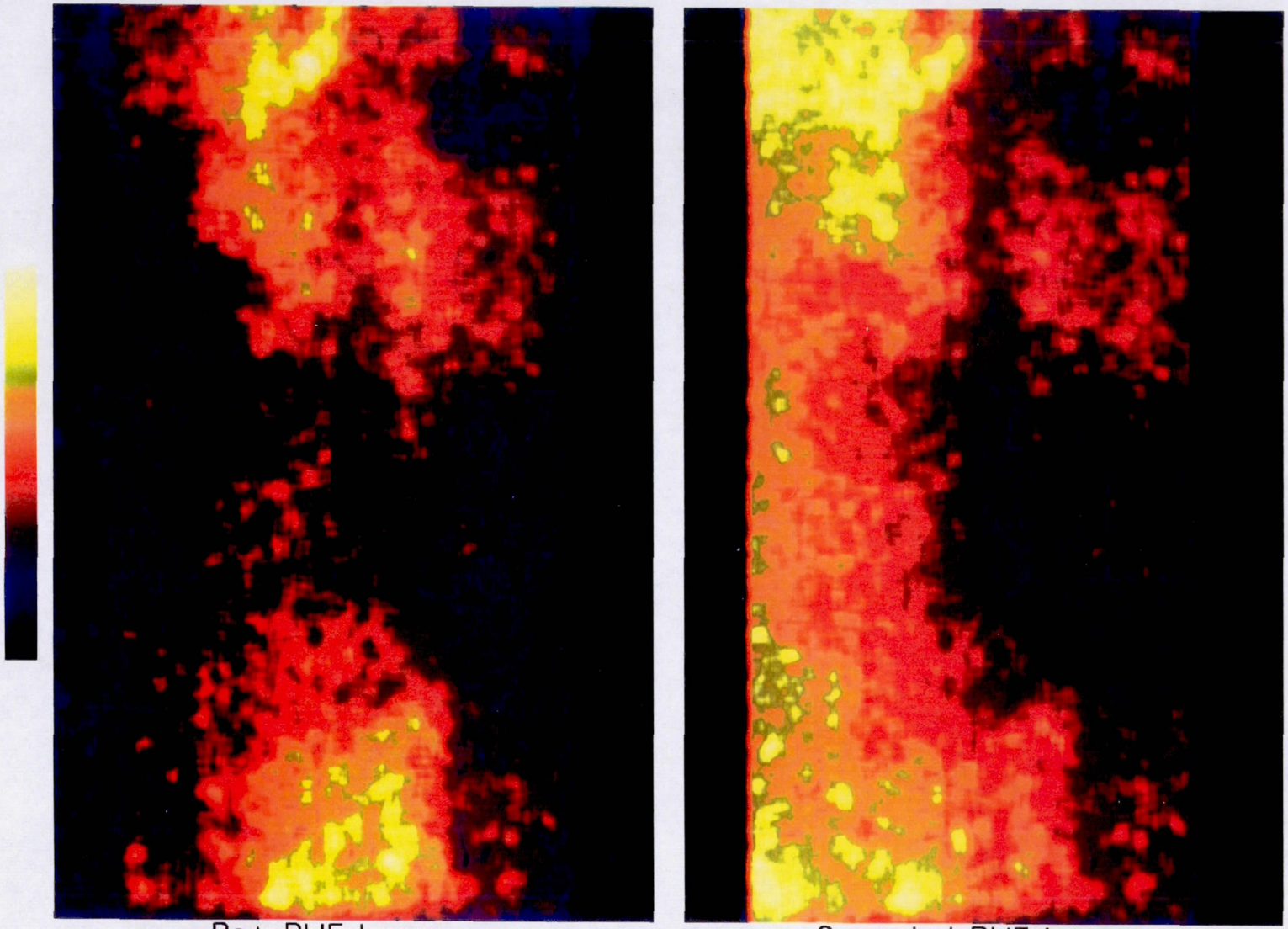

Fig. 5 Comparison of uncorrected and corrected single shot OH PLIF images for 9-pt LDI with 45° swirl, at 150 psia and Φ=0.53. Resonant excitation is $R_1(10)$.

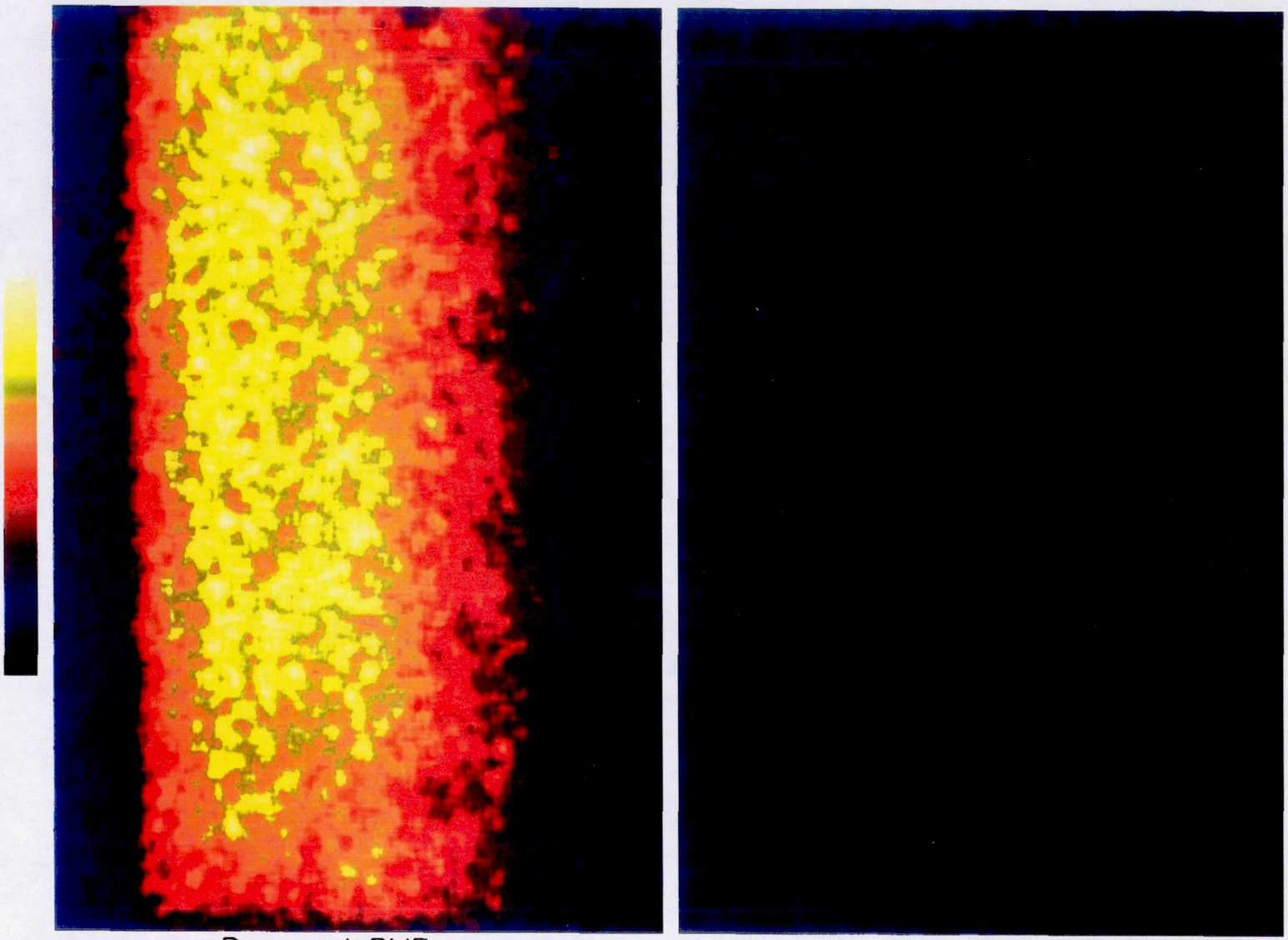

Fig. 6 Comparison of resonant and non-resonant OH PLIF images for 9 pt LDI with 60°/45° swirl at 150 psia and Φ = 0.53. Resonant excitation is $R_1(10)$.

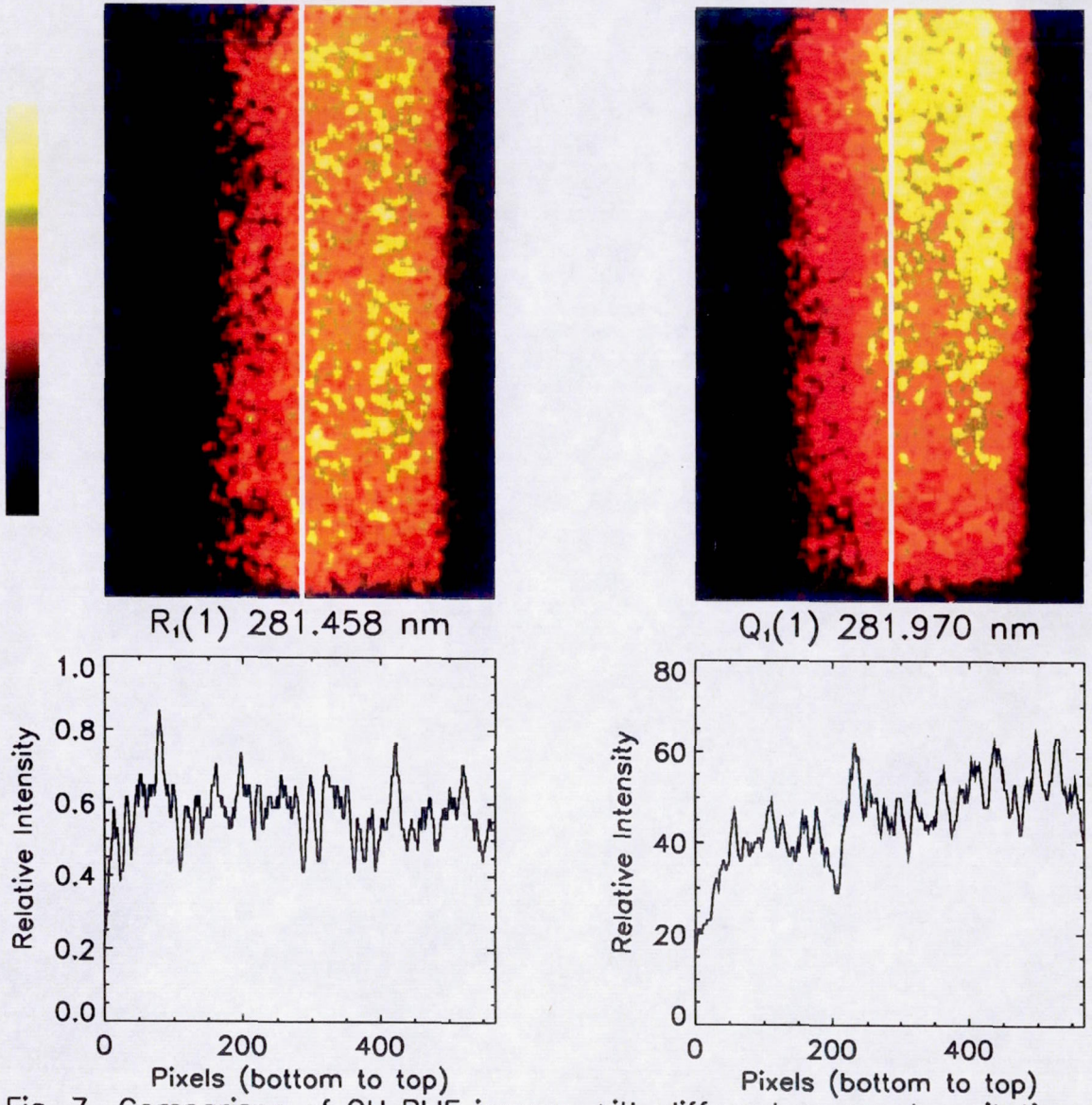

Fig. 7 Comparison of OH PLIF images with different resonant excitation for 9 pt LDI with 60°/45° swirl at 150 psia and Φ = 0.53.

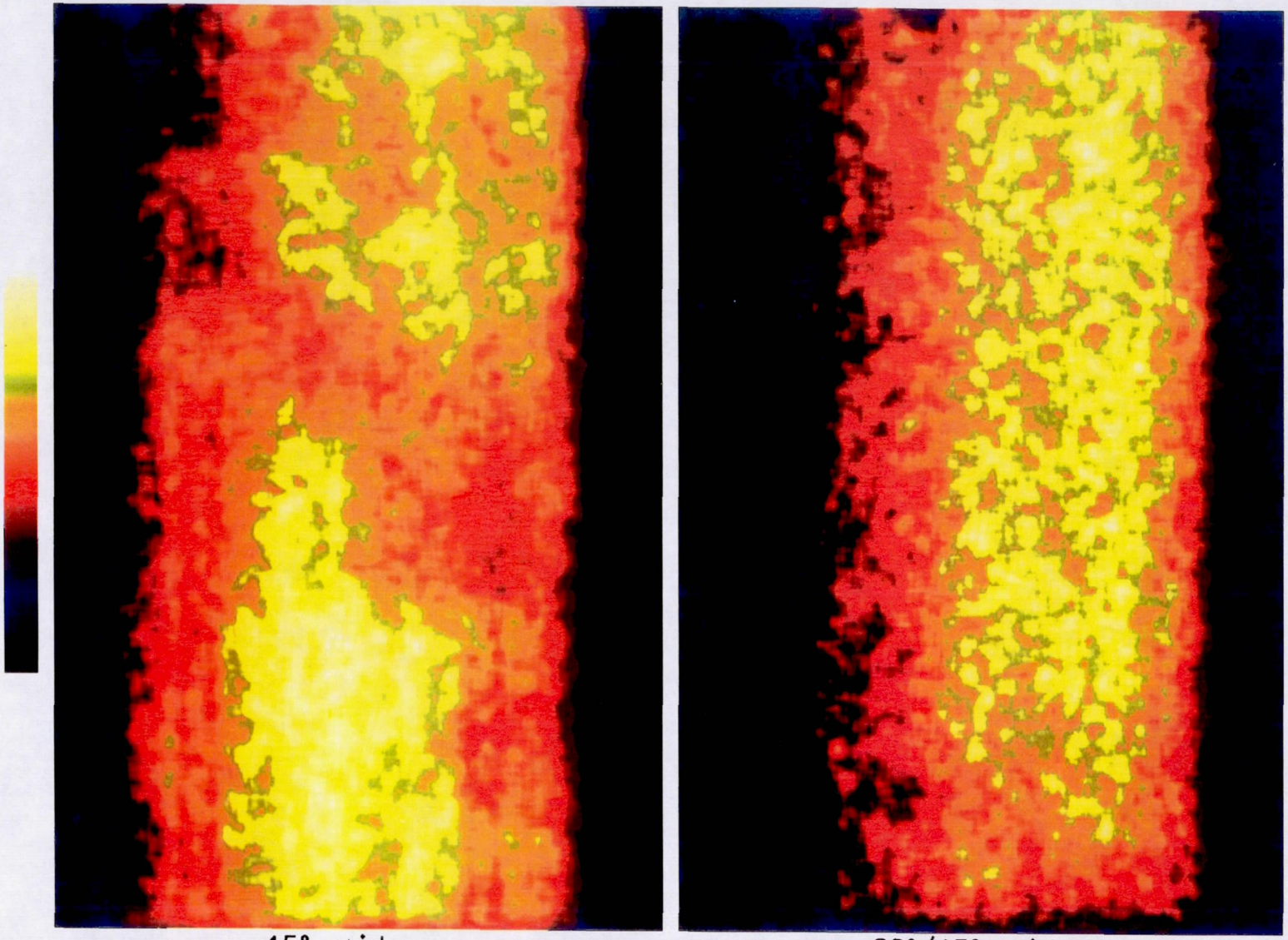

Fig 8. Comparison of OH PLIF images for different fuel injector configurations with 9 pt LDI at 150 psia and Φ = 0.53. Resonant excitation is $R_1(10)$.

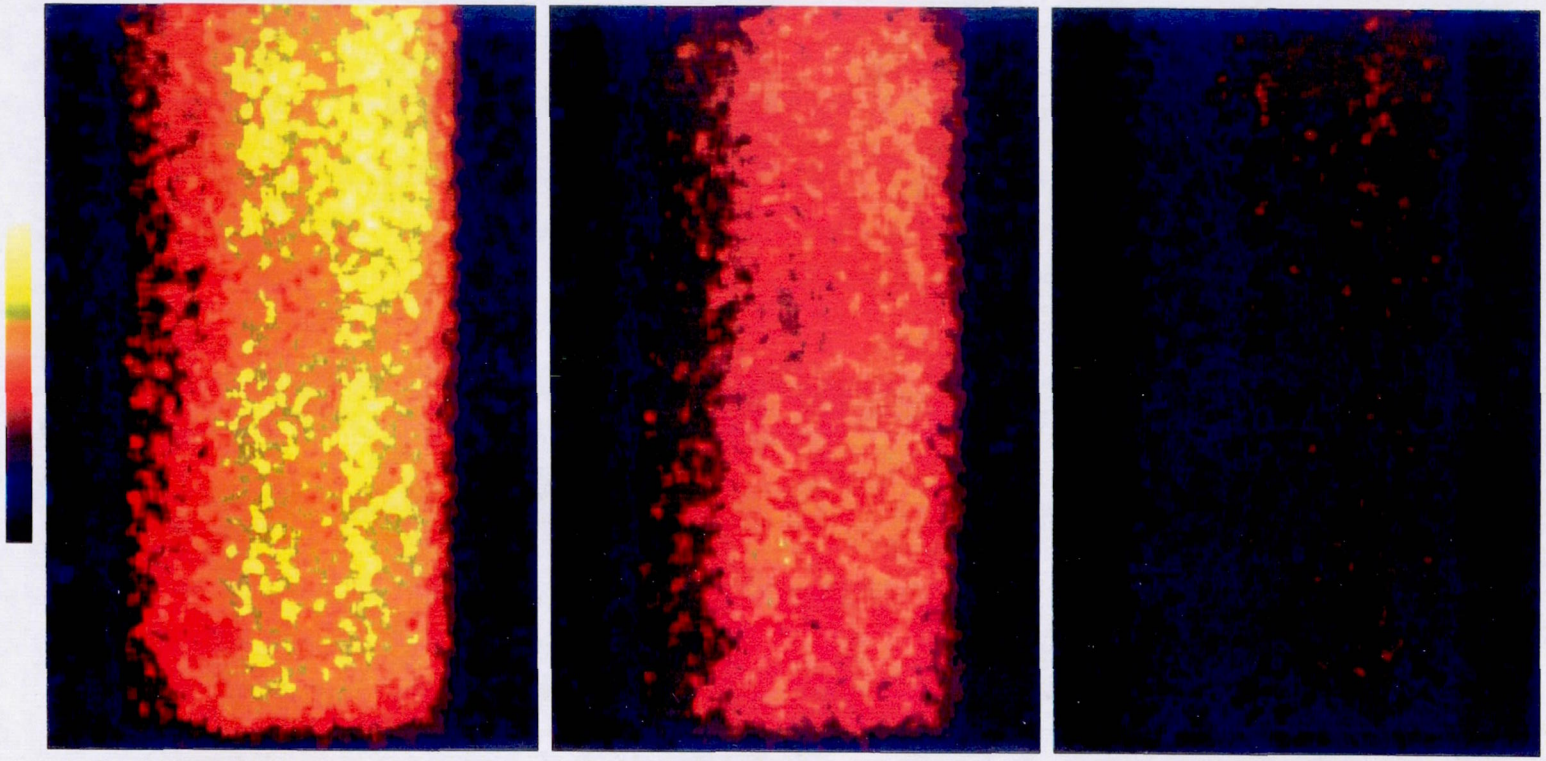

Φ = 0.53 Φ = 0.47 Φ = 0.41

Fig. 9 Comparison of OH PLIF images for different equivalence ratios at 205 psia with 9 pt LDI with 60°/45° swirl. Resonant excitation is $R_1(10)$.

REPORT DOCUMENTATION PAGE

Form Approved
OMB No. 0704-0188

1. AGENCY USE ONLY (*Leave blank*)	2. REPORT DATE	3. REPORT TYPE AND DATES COVERED
	February 1995	Technical Memorandum

4. TITLE AND SUBTITLE

Two-Dimensional Imaging of OH in a Lean Burning High Pressure Combustor

5. FUNDING NUMBERS

WU–537–02–21

6. AUTHOR(S)

R.J. Locke, Y.R. Hicks, R.C. Anderson, K.A. Ockunzzi, and G.L. North

7. PERFORMING ORGANIZATION NAME(S) AND ADDRESS(ES)

National Aeronautics and Space Administration
Lewis Research Center
Cleveland, Ohio 44135–3191

8. PERFORMING ORGANIZATION REPORT NUMBER

E–9444

9. SPONSORING/MONITORING AGENCY NAME(S) AND ADDRESS(ES)

National Aeronautics and Space Administration
Washington, D.C. 20546–0001

10. SPONSORING/MONITORING AGENCY REPORT NUMBER

NASA TM–106854
AIAA–95–0173

11. SUPPLEMENTARY NOTES

Prepared for the 33rd Aerospace Sciences Meeting and Exhibit sponsored by the American Institute of Aeronautics and Astronautics, Reno, Nevada, January 9–12, 1995. R.J. Locke, NYMA, Inc., Engineering Services Division, 2001 Aerospace Parkway, Brook Park, Ohio 44142 (work funded by NASA Contract NAS3–27186); Y.R. Hicks and R.C. Anderson, NASA Lewis Research Center; K.A. Ockunzzi, Ohio Aerospace Institute, 22800 Cedar Point Road, Cleveland, Ohio 44142; G.L. North, Vehicle Propulsion Directorate, U.S. Army Research Laboratory, NASA Lewis Research Center. Responsible person, Y.R. Hicks, organization code 2710, (216) 433–3410.

12a. DISTRIBUTION/AVAILABILITY STATEMENT

Unclassified - Unlimited
Subject Categories 07 and 35

This publication is available from the NASA Center for Aerospace Information, (301) 621–0390.

12b. DISTRIBUTION CODE

13. ABSTRACT (*Maximum 200 words*)

Planar laser-induced fluorescence (PLIF) images of OH have been obtained from an optically accessible, lean burning high pressure combustor burning Jet-A fuel. These images were obtained using various laser excitation lines of the OH A←X (1,0) band for several fuel injector configurations with pressures ranging from 1013 kPa (10 atm) to 1419 kPa (14 atm). Non-uniformities in the combusting flow, attributed to differences in fuel injector configuration, are revealed by these images. Contributions attributable to fluorescent aromatic hydrocarbons and complex fuel chemistries are also not evident.

14. SUBJECT TERMS

Laser diagnostics; LIF; PLIF flow visualization; Lean-burn combustion; Species distribution

15. NUMBER OF PAGES
21

16. PRICE CODE
A03

17. SECURITY CLASSIFICATION OF REPORT	18. SECURITY CLASSIFICATION OF THIS PAGE	19. SECURITY CLASSIFICATION OF ABSTRACT	20. LIMITATION OF ABSTRACT
Unclassified	Unclassified	Unclassified	